Frictional dynamics of finger pads are governed by four length-scales and two time-scales*

Brygida Dzidek, Séréna Bochereau, Simon Johnson, Vincent Hayward and Michael Adams

Abstract—The evolution of the contact area of a finger pad against a surface is critical during tactile interaction, whether for gripping or discriminating surfaces. The contact area made by a finger pad is commonly considered at two distinct length scales corresponding to the gross area, A_{gross}, and to the smaller ridge area, A_{ridge}, that excludes the interstitial spaces between the ridges. Here, these quantities were obtained from high-resolution imaging of contacts during loading and stress relaxation. While A_{gross} rapidly reaches an ultimate value, the contact made by the ridges is initially formed from unconnected junctions with a total contact area, A_{junct}, which continues to increase for several seconds during the holding period. Thus, the contact area grows in a two-step process where the number of junctions made by the ridges first increases, followed by a growth of their size and connectivity. Immediately after contact the *stratum corneum* is in a glassy state and the individual junctions form a multiple asperity contact. At longer contact times, the asperities soften owing to the occlusion of moisture excreted from the sweat pores in the ridges. Thus, the real area of contact, A_{real}, which drives the creation of friction, grows with time at a relatively slow rate. It is concluded that multi-asperity dynamic contact models should be preferred compared with static models in order to describe the physics of finger pad contact mechanics and friction.

I. INTRODUCTION

Grip and touch are mediated through finger pads. While a detailed knowledge of the biotribology of fingertips is fundamental to studies of gripping behaviour and discriminative touch, this knowledge has gained additional importance with the recent advent of tactile displays that depend on the modulation of fingertip friction to operate.

The finger pad is a complex mechanical structure that is adapted to interact with a large range of materials under varied loading and environmental conditions. It comprises several layers of different tissues each endowed with particular properties [1]. The outer layer that comes in direct contact with objects, the *stratum corneum*, possesses specific permeation properties rendering the physical chemistry of

this material highly sensitive to the presence of water [2]. The fingerprint ridges, furrows, and sweat pores are the visible macroscopic features of this structure. Prior studies have shown that the ridges are far from being smooth but exhibit smaller scale asperities [3].

A detailed understanding of the complexities of fingerprint deformation is necessary to address the mechanisms by which humans discriminate surfaces and grip objects. However, most studies tend to neglect the complexity of the finger pad topography, using instead a bulk approach [4]. As it turns out, we have found in the present study that smaller scale contact mechanics may in fact dominate over gross effects in the finger pad interaction with objects.

There are many sweat pores in the finger print ridges. During sustained contact with an impermeable smooth surface, the secreted moisture softens the ridges by plasticisation thus inducing a glassy-rubbery transition; this occlusion mechanism results in a large increase in the contact area and hence the friction as discussed below [2]. The temporal evolution of friction can be described by an empirical, first-order kinetics relationship,

$$\mu = \mu_\infty + (\mu_0 - \mu_\infty) \exp(-t/\lambda_1), \qquad (1)$$

where μ is the coefficient of friction, the subscripts 0 and ∞ refer to the initial and asymptotic values, t is time, and λ_1 is the characteristic time. The increase in friction is surprisingly slow with $\lambda_1 \sim 20$ s for optically flat glass. The width, height, and length of each ridge change considerably when stressed in shear or compression [5]. Shearing loads can lead to gross deformation of 100% without damage [6], with small bumps inducing 30% deformation [7]. A water-bed model, [8], could be made to match empirical data under canonical, gross loading conditions.

At a smaller scale, Bhushan [9] applied a multiple asperity contact model proposed earlier by Greenwood & Williamson in [10] for nominally flat elastic bodies. In this model, the sum of the areas of all the individual contacts constitutes the real (true) area of contact. Deformation occurs in the regions of asperity contact, establishing stresses that oppose the applied load. With increasing applied load, the number of asperities and the size of their contact spots increase. Hence, surfaces may be viewed to be composed of features at multiple length scales of roughness that are superimposed on each other [11]. A number of studies have examined the influence of the topography of counter-surfaces on the friction of the finger pad [12]. For regular counter surface textures, it was observed that the coefficient of friction increased with the tip radius and number density of the asperities as would be expected by the resulting increase in the real area of contact [3].

Brygida Dzidek and Michael Adams are with the School of Chemical Engineering, University of Birmingham, Birmingham B15 2TT, UK (e-mail: m.j.adams@bham.ac.uk).

Séréna Bochereau and Vincent Hayward are with Sorbonne Universités, Université Pierre et Marie Curie Paris 06, Unité Mixte de Recherche 7222, Institut des Systèmes Intelligents et de Robotique, 75005 Paris, France (e-mail: vincent.hayward@isir.upmc.fr).

Simon Johnson is with Unilever R&D Port Sunlight, Bebington, Wirral CH63 3JW, UK (e-mail: simon.johnson@unilever.com).

Warman & Ennos [4] examined the effects of fingerprints on friction with a view to explaining their function. They argued that they could improve grip by (a) inducing interlocking on rough counter-surfaces, (b) allowing excess water to escape, (c) acting as part of highly deformable structure to maximise the contact area at small forces and (d) allowing greater normal forces to be applied without damaging the skin. Currently, direct experimental evidence is not available to support these possible mechanisms.

Frictional effects are fundamental during texture discrimination tasks and are directly related to the contact area. The adhesion model of friction [13] is applicable to skin and is such that $F = \tau A_{\text{real}}$ where F, τ, and A_{real} are respectively the frictional force, the interfacial shear strength, and the real contact area [14]. For multiple asperity (rough) junctions, A_{real} is to a first approximation proportional to the normal load, W, hence the friction is Coulombic with $F = \mu W$. For sphere-on-flat (point) or cylinder-on-flat (line) Hertzian junctions, A_{real} is proportional to $W^{2/3}$ or $W^{1/2}$, respectively, so that the frictional force is modelled by $F = kW^n$ where $n = 2/3$ or $1/2$ provided that the dependence of τ on the contact pressure is small; n is termed the *frictional load index* [14]. For contacts of the finger pad, which generally are strongly time-dependent, we observed in the case of an occlusive contact that $n \sim 1$ initially and that it decreased with sliding time to reach a value of $\sim 2/3$ [15]. Similarly to (1), the temporal dynamics could be described empirically by a first-order kinetics relationship,

$$n(t) = n_\infty + (n_0 - n_\infty) \exp(-t/\lambda_1). \qquad (2)$$

In the previous literature, two measures of the contact area are generally encountered, namely, the gross value, A_{gross}, which is the total area contained within the overall contact boundary, and the value associated with the ridges, A_{ridge}, which is based on the contact area of the ridges as defined by their gross contact boundaries. In previous works, it is typically assumed that A_{ridge} approximates A_{real}. Warman & Ennos, [4], using ink prints to estimate A_{ridge}, found that the ratio $A_{\text{ridge}}/A_{\text{gross}}$ was ~0.7 but was very sensitive to load. Childs & Henson [16], using an optical method, reported that this ratio was indeed clearly load-dependent with values of 0.12, 0.23, and 0.34 for loads of 0.41, 0.88, and 1.77 N. These results are reasonably consistent with those of Soneda & Nakano [17], who also used an optical method to report that this ratio increased with increasing normal load such that its value was 0.3 at 1.0 N. Moreover, for the fully occluded state at long contact times, it was observed that A_{ridge} increased with load according to the Hertz equations with an areal load index of 2/3. However, the value of A_{gross} was associated with a smaller index of 0.52. It thus appears that A_{ridge} increases faster with the normal load than does A_{gross}, a phenomenon also reported by others [18,19].

In order to estimate the load index of A_{gross} in the fully occluded state, it is reasonable to assume that the fingertip contact can be approximated by an elliptical Hertzian geometry [20]. In addition, the asymptotic areal load index of A_{ridge} in the fully occluded state can be estimated by representing the ridges by Hertzian line contacts. In the initial glassy state, a multiple asperity contact is created because the hard asperities do not deform sufficiently to form a smooth interface. The origin of this asperity persistence has still to be clarified but could involve such factors as the interaction of neighbouring sub-surface stress fields. There are rigorous models of multiple asperity contacts for specific surface topographies, e.g. [21], but the Archard model [22] is conceptually most useful. It considers spherically-capped Hertzian asperities that are such if their number remains constant with increasing load, then $n = 2/3$; but if the number increases with load, then $n \to 1$. One of the aims of the current work was also to understand the contact mechanics consequences of the glassy-rubbery state transition, also known as the Archadian-Hertzian transition, induced by occlusion. To this end, we imaged the fingerprint contact using a high-resolution optical method in order to delineate the characteristic length and time scales of an occluding contact. It was observed that the contact of the ridges was not continuous but that small junctions were formed, which were associated at a small length scale with a newly defined contact area, A_{junct}.

II. METHODS

A. Apparatus

The experimental platform used to measure the time evolution of the contact area and the deforming load is shown in Fig. 1. The left index finger of a female volunteer (27 years old) was inclined at 30° with the finger pad facing upwards. A right-angle prism was attached to the loading platform of a universal mechanical testing machine (model no. 5566, Instron, High Wycombe, UK) fitted with a 10 N load transducer. The flat glass prism was pressed down onto the finger pad in order to induce frustrated total internal reflection while the contact area increased with applied load.

Figure 1. Schematic diagram showing the prism-based imaging method. The prism attached to the loading platform was pressed onto the finger pad. The dorsal side of the finger was secured on an angled block by double-sided adhesive tape.
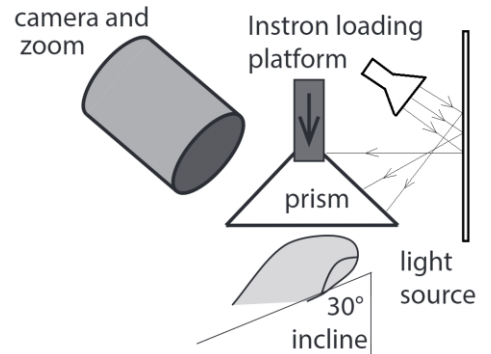

The image resulted in a high-contrast pattern of dark ridges where the light was scattered and a bright background where

the light was completely reflected. The finger pad compression was effected at a rate of 1 mm/s until a load of 2 N was reached. At this point, the prism movement was halted for 10 s before unloading the contact at the same rate. The finger had been washed with commercial soap, rinsed with distilled water and left to dry for 10 min until an equilibrated clean skin state was reached. All measurements were carried out in an environmentally controlled laboratory set to 20°C and 50% relative humidity.

The rear face of the prism was backlit uniformly by reflecting light from a fibre-optic lamp with a diffusely reflecting white surface. The contact was imaged through the front face of the prism using a Nikon D5000 camera with a video resolution of 1280 x 720 pixels at 24 fps and a shutter speed of 1/200 s. The camera was fitted with a macro lens and a small aperture was used to achieve the depth of field necessitated by oblique viewing.

B. Image Analysis

Figure 2. Image of the finger pad at a load of 2 N. The ridges were thicker and darker at the centre, compared to those at the periphery, corresponding to the greater pressure. The zoomed in rectangular area shows the sweat pores as white circular regions.
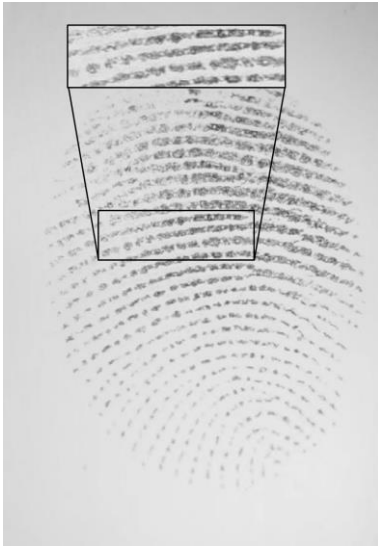
Using the ImageJ software, image analysis was carried out to determine A_{gross}, A_{ridge}, and A_{junct} as a function of the contact duration. Basic grey scale (8-bit) conversion and analysis was applied to 672 frames. The converted images were adjusted to the level of contrast and brightness that allowed for optimal pattern recognition. The values of A_{gross} were determined manually by fitting the peripheral border. To speed up the fitting process, the analysis was performed every 20th frame during the two second loading period and every 40th frame during the holding period. The value of A_{ridge} was determined from the value that was enclosed by the gross boundary, which included the spaces between the junctions due to the sweat pores, by interactively setting lower and upper threshold values. Low or uneven

connectivity on the periphery was enhanced but remained unconnected. Typical methods were adopted for automatic fingerprint feature extraction [23] and follow a sequence of steps comprising image enhancement, binarisation, thinning, extraction, and post-processing. It was possible to exclude pores and to determine the size and evolution of each feature by segmenting the image into features of interest from the background under each relevant condition by use of a mask function. To estimate A_{junct}, a threshold grey scale value was determined from a histogram of the pixel intensities that allowed the boundaries of the contact junctions to be delineated. The boundary of each junction included sweat pores at the edge of the contact region but it was not possible to automatically exclude those that were internal to the boundaries. It was calculated that the overestimate of the contact area was < 5% since such internal sweat pores represented a relatively small proportion of the total contact area particularly since they were only present in the central region of the finger pad image.

III. RESULTS

An unprocessed image of the finger pad contact is shown in Fig. 2. The darker regions are larger in the central zone of the gross contact. The small white circles within the contact junctions as well as the gaps along the ridges arise from the presence of the sweat pores. The zoomed-in region shows more clearly the disconnected nature of the ridges. Figure 3(a) shows enlarged regions to exemplify the increase in size and connectivity of the junctions over the loading and hold periods. The size and connectivity of these junctions were greater in the central zone compared to the peripheral region. Figures 3(b) and (c) show the contour plots of the fingerprint images at 2 and 11 s from contact onset.

Figure 3. (a) Local binary mask of the junctions over the test period. Contact contour images at (b) the end of the 2 s loading period and (c) at the end of the 11 s hold period.
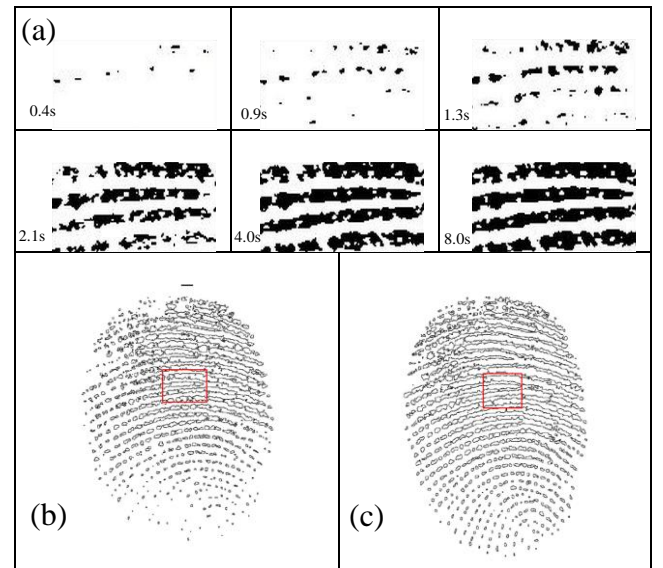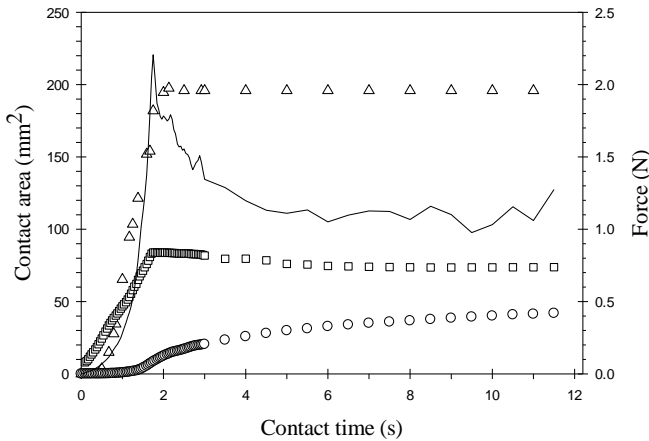
Figure 4 plots the normal force evolution as a function of time, showing and increase during the loading period and stress relaxation during the holding period. The trajectory of A_{gross} as a function of time shows that it reaches a maximum value just after loading and remains constant during the holding period. Figure 4 also includes a plot of the total area of the junctions, A_{junct}. There is a progressive augmentation of this value during the initial phase of the loading period, but A_{junct} continues to grow throughout the entire holding period. In the meantime, A_{ridge} exhibits values that are between the commonly assumed values and those presently observed for A_{junct}. The asymptotic ratio $A_{\text{ridge}}/A_{\text{gross}}$ is about 0.39, which is consistent with the values previously reported [18].

Figure 5 reports the temporal evolution of the number of junctions, N_c. Most were formed during the loading period. The value of N_c decreases only slightly during the holding period because, although there is coalescence of some junctions in the central region, this is compensated by the formation of new junctions in the peripheral region. The junction density, N_c/A_{gross}, first decreases dramatically and then slowly creeps down because the rate of increase of A_{gross} is slightly greater than that of N_c.

Figure 4. Temporal evolution of A_{gross} (Δ), A_{ridge} (□), A_{junct} (○) and load (-) during finger pad compression.

plasticised by the transport of moisture from the sweat pores and expand owing to material softening.

A moderate increase in connectivity in the central region where junction growth is greatest can be observed. Plasticisation of the *stratum corneum* by moisture softens the asperities causing existing junctions to progressively form more intimate contacts. Consequently, as A_{gross} grows, the value of n reduces. The existing junctions grow but the peripheral regions of the gross contact become populated by non-plasticised asperities, causing the new contacting asperities to form a multiple-asperity region with n equal to one. At longer time scales, the proportion of peripheral areas exhibiting multiple asperity contacts eventually vanish and thus $n \to 2/3$.

Figure 5. Number of junctions, N_c, as a function of contact time (continuous line) compared with the number density, N_c/A_{gross} (□).
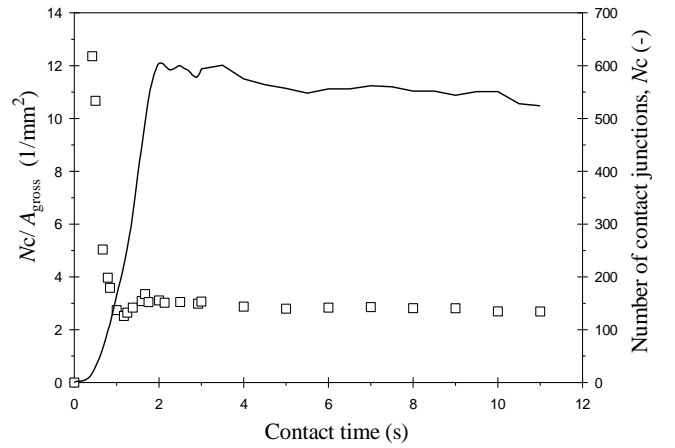

Figure 6 shows how A_{junct} evolves as a function of time. On the basis of (1), the data from the hold period can be fitted with a first order kinetics relationship,

$$A_{\text{junct}} = A_{\text{junct,0}} + \left[A_{\text{junct,0}} - A_{\text{junct,}\infty}\right] \exp\left\{-\frac{(t+t_*)}{\lambda_2}\right\}, \quad (3)$$

where here t represents the measured time after initial contact. However, the load was not applied instantaneously and it is necessary to add an additional time period, $t_* = 1.7$ s, that satisfies the boundary condition $A_{\text{junct}} = A_{\text{junct,0}} = 0$ at $t + t_* = 0$. The best fit of (3) to the data is shown in Figure 6 corresponding to $A_{\text{junct,}\infty} = 50.5 \pm 0.7$ mm^2. Interestingly, λ_2 is 7.1 ± 0.2 s, which is considerably shorter than the value of 18 ± 5 s for λ_1, which is the characteristic time for the increase in friction of the same finger on glass [15]. This result implies that the growth rate of A_{junct} is significantly greater than that of A_{real}. Thus, overcoming asperity persistence is significantly more difficult than the gross deformation of the junctions.

Given that the asymptotic value of A_{gross} is 195.8 mm^2, $\left(A_{\text{junct}}/A_{\text{gross}}\right)_\infty = 0.26$. Consequently, if it assumed that the asymptotic value of $A_{\text{real}} = A_{\text{junct}}$, then the real area of contact at long occlusion times is about one quarter of the

IV. DISCUSSION

The finger print ridges are punctuated by sweat pore openings with trumpet bell profiles. These concavities have a reported average peripheral diameter of 109 μm, and an average separation between them on one ridge of 390 μm [24]. As discussed previously, the frictional load index, n, is about unity at contact onset. Thus, the junctions in the hinterlands between the sweat pores correspond, at short times, to multiple asperity contacts since the *stratum corneum* is in a glassy state. The increase of A_{junct} with load in the initial phase of a contact is thus mostly due to an increase of the number of junctions, N_c, rather than an increase in their size. At longer times, the junctions become

gross area and will be considerably less at shorter dwell times. It should be emphasised this is a result from limited measurements at a single normal load and for a single subject, but the general behaviour is expected to be applicable irrespective of the loading and subject.

The conventional assumption that $A_\text{real} = A_\text{ridge}$ has arisen from the use of ink for real contact visualisation or from imaging without sufficient resolution. The present images are consistent with those reported by Childs & Henson [16], but perhaps because of the poor quality of the ink print images, their significance was under-appreciated.

Figure 6. The best fit of Eq. (3) to the measured values of A_junct as a function of $(t + t_*)$.
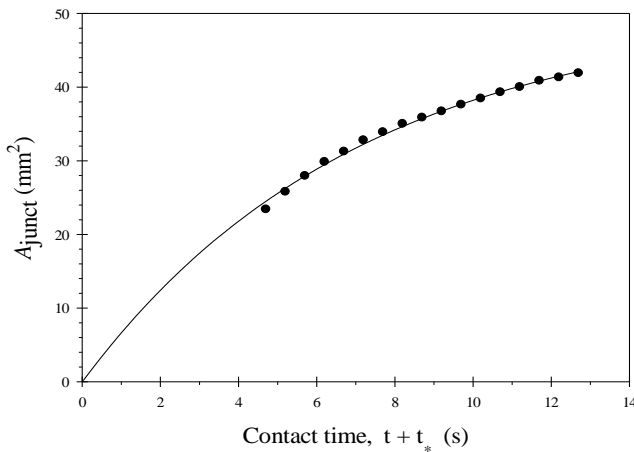
Our results also indicate that friction, driven by the growth dynamics of the real area of contact, may play a determining role in the perception of roughness, slipperiness, and warmth, as recently reviewed in reference [12].

Some tactile displays rely on decreasing friction by ultrasonic vibration of a smooth counter surface [25-27]. It has been shown that the modulation of friction could be explained partially by repeated collisions of the counter-surface with the finger pad [28]. This finding is supported by the fact that at the length scale of the asperities (of the order of microns), exposure to air could lead to drying and de-plasticisation. Consequently, asperity persistence could be an essential contributory factor to friction reduction, thus providing a possible explanatory mechanism for the observed phenomenon.

V. Conclusion

In summary, the present work has shown that four characteristic length scales, rather than just two as previously assumed, are required to describe the contact mechanics of the finger pad; namely those associated with the gross finger geometry, the ridges, the junctions, and the asperities within the junctions. In addition, there are two characteristic times respectively associated with the growth rates of the junctions and of the real contact areas. These length and time scales are important in understanding how the Archardian-Hertzian transition drives both the large increase of friction and the

reduction of the areal load index during persisting finger contacts with impermeable surfaces.

It is probable that because of the microscopic length scale of the ridge asperities, de-plasticisation takes place during intermittent contacting caused by ultrasonically vibrating surfaces employed in some tactile displays, enhancing persistence and thus contributing to a reduction in friction.

Moreover, our findings demonstrate that the growth of the contact area results from a two-step mechanism, with some correlation between the steps. The growth of A_gross is initially due to the recruitment of ridge apices interacting with the surface during initial loading. The second step is associated with the contributions of peripheral ridges progressively making contact with the counter-surface to form isolated junctions. With increasing load, the number, size, and connectivity of these junctions all grow simultaneously. Initially, *stratum corneum* is in a glassy state so that each junction forms a Coulombic multiple-asperity contact. With the onset of plasticisation due to the trapping of moisture in the junctions, the asperities become softer, but with a characteristic time that is significant longer than that corresponding to junction growth itself.

These findings imply that multiple asperity contact might play a key role in vibration-based tactile stimulation devices. The rendering of tactile sensation could be more realistic if the contact area and pressure distribution of the finger experiencing the device was measured to adapt the stimuli in real time against varying ambient or physiological conditions. Such corrective actions would be feasible since a few seconds are required for full plasticisation and for the formation of intimate contacts.

Texture appreciation and shape discrimination also rely on frictional dynamics since they can be expected to depend on the microscopic features of finger pads. This is because finger pads should be considered as rough surfaces at the small scales at play during short frictional interactions. In the case of an interaction with rough counter surfaces, occlusion is reduced or even absent. For example, with sufficient surface roughness, the coefficient of friction ceases to increase with contact duration [15]. Thus, if we consider a finger sliding over rough surfaces, the rough-rough contacts are likely to influence the spectral content of the vibrations generated by the contact, thus modifying the tactile experience.

Tactile interactions involving relatively short times scales are more easily accomplished if friction is small. However, precision tasks and object gripping *per se* generally require long dwell times and are facilitated by the relatively high friction induced by the plasticisation of the asperities according to the degree of roughness and permeability of the counter-surfaces.

References

[1] M. Geerligs, C. W. J. Oomens, P. A. J. Ackermans, F. P. T. Baaijens and G. W. M. Peters, "Linear shear response of the upper skin layer," *Biorheology*, vol 48, pp. 229–245, 2011.

[2] S. M. Pasumarty, S. A. Johnson, S. A. Watson and M. J. Adams, "Friction of the human finger pad: influence of moisture, occlusion and velocity," *Tribol. Lett.*, vol. 44, no. 2, pp. 117–137, 2011.

[3] J. van Kuilenburg, M. A. Masen and E. van der Heide, "The role of the skin microrelief in the contact behavior of human skin: Contact between the human finger and regular surface textures," *Tribol. Int.*, vol. 65, pp. 81–90, 2013.

[4] P. H. Warman and A. R. Ennos, "Fingerprints are unlikely to increase the friction of primate fingerpads," *J. Exp. Biol.*, vol. 212, no. 13, pp. 2016–2022, 2009.

[5] Q. Wang and V. Hayward, "In vivo biomechanics of the fingerpad skin under local tangential traction," *J. Biomech.*, vol. 40, no. 4, pp. 851–860, 2007.

[6] V. Levesque and V. Hayward, "Experimental evidence of lateral skin strain during tactile exploration," *Proc. Eurohaptics Conf.*, pp. 261–275, 2003.

[7] M. A. Srinivasan "Surface deflection of primate fingertip under line load," *J. Biomech.*, vol. 22, no. 4, pp 343–349, 1989.

[8] M. A. Srinivasan, and K. Dandekar, "An investigation of the mechanics of tactile sense using two-dimensional models of the primate fingertip," *J. Biomech. Eng.*, vol. 118, no. 1, pp. 48–55, 1996.

[9] B. Bhushan, "Contact mechanics of rough surfaces in tribology: multiple asperity contact," *Tribol. Lett.*, vol. 4, pp. 1–35, 1998.

[10] J. A. Greenwood and J. B. P. Williamson, "Contact of nominally flat surfaces," *Proc. Roy. Soc. London A,* vol. 295, pp. 300–319, 1966.

[11] A. Majumbar and B. Bhushan, "Role of fractal geometry in roughness characterization and contact mechanics of rough surfaces," *ASME J. Tribol.*, vol. 112, pp. 205–216, 1990.

[12] J. van Kuilenburg, M. A. Masen and E. van der Heide, "A review of fingerpad contact mechanics and friction and how this affects tactile perception," *Proc. IMechE, Part J,* vol. 229, no.3, pp.243–258, 2013.

[13] F. P. Bowden and D. Tabor, "Friction and Lubrication of Solids," *Oxford University Press*, London, 1954.

[14] M. J. Adams, B. J. Briscoe and S. A. Johnson, "Friction and lubrication of human skin," *Tribol. Lett.*, vol. 26, no. 3, pp. 239–253, 2007.

[15] B. M. Dzidek, M. J. Adams, Z. Zhang, S. Johnson, S. Bochereau, and V. Hayward, "Role of occlusion in non-Coulombic slip of the finger pad," *Haptics: Neuroscience, Devices, Modeling, and Applications,* Springer Berlin Heidelberg, pp. 109–116, 2014.

[16] T. H. C. Childs and B. Henson, "Human tactile perception of screen-printed surfaces: Self-report and contact mechanics experiments," *Proc. IMechE, Part J*, vol. 22, no. 3, pp. 427–441, 2007.

[17] T. Soneda and K. Nakano, "Investigation of vibrotactile sensation of human fingerpads by observation of contact zones," *Tribol. Int.*, vol. 43, no. 1, pp. 210–217, 2010.

[18] X. Liu, Z. Lu, R. Lewis, M. J. Carré and S. J. Matcher, "Feasibility of using optical coherence tomography to study the influence of skin structure on finger friction," *Tribol. Int.*, vol. 63, pp. 34–44, 2013.

[19] S. E. Tomlinson, R. Lewis, M. J. Carre and S.E. Franklin, "Human finger friction in contacts with ridged surfaces," *Wear*, vol. 301, no. 1, pp. 330–337, 2013.

[20] B. M. Dzidek, M. Adams, J. W. Andrews Z. Zhang, S. Johnson, "Contact mechanics of the human finger pad under compressive loads," in preparation, 2016.

[21] K. L. Johnson, "Contact mechanics," *Cambridge University Press*, Cambridge, UK, 1985.

[22] J. F. Archard, "Elastic deformation and the laws of friction," *Proc. Roy. Soc. London A*, vol. 243, no. 1233, pp. 190–205, 1957.

[23] C. Domeniconi, S. Tari, and P. Liang, "Direct gray scale ridge reconstruction in fingerprint images," *IEEE ICASSP*, pp. 2941–2944, 1998.

[24] A. R. Roddy, J. D. Stosz, "Fingerprint features—statistical analysis and system performance estimates," *Proc. IEEE*, vol. 85, no. 9, pp. 1390–1421, 1997.

[25] T. Watanabe and S. Fukui, "A method for controlling tactile sensation of surface roughness using ultrasonic vibration," *IEEE Int. Conf. Robotics and Automation*, vol. 1, pp. 1134–1139, 1995.

[26] M. Biet, F. Giraud, B. Lemaire-Semail, "Squeeze film effect for the design of an ultrasonic tactile plate," *IEEE Trans. Ultrason. Ferroelect. Freq. Control*, vol. 54, no. 12, pp. 2678–2688, 2007.

[27] L. Winfield, J. Glassmire, J. E. Colgate, M. Peshkin, "T-pad: Tactile pattern display through variable friction reduction," *Proc. World Haptics Conf.*, pp. 421–426, 2007.

[28] E. Vezzoli, B. M. Dzidek, T. Sednaoui, F. Giraud, M. J. Adams, B. Lemaire-Semail, "Role of fingerprint mechanics and non-Coulombic friction in ultrasonic devices," *Proc. World Haptics Conf.*, 2015.